Nanoscale Advances **Review Article**

Electronic Supplementary Information (ESI)

Ecofriendly Ruthenium Containing Nanomaterials: Synthesis, Characterization, Electrochemistry, Bioactivity and Catalysis

Pranshu K. Gupta and Lallan Mishra*

**Department of Chemistry, Institute of Science, Banaras Hindu University, Varanasi-221005*, India, lmishrabhu@yahoo.co.in

Contents or Supplementary Description (SD):

Abbreviations:

Angio.: Angiosperms, **Gymno.**: Gymnosperm, **Pteridо.**: Pteridophyte, **G-**: Gram-negative, **N/D**: Not Defined, **RT**: Room Temperature, **MD**: Monodispersed, **PD**: Polydispersed, **BTC**: Benzene to cyclohexane, **MTS**: Maleic acid to succinic acid, **NTA**: Nitro to amino, **MFC**: Methanol Fuel Cell, **NC**: Nanocatalysts, **SF**: Semi Fermented, **@(stir):** Activated by stirring, **@**: at/over, **NiF**: Ni foam, **BD**: Bulk Density, **P**: Porosity, **Avg**.: Average, **Ext**.: Extract, **Soln.**: Solution, **TOF**: Turn Over Frequency, **HERE**: Hydrogen Evolution Reaction Efficiency, **Op**: Overpotential, **CD**: Current Density, **ER**: Efflux Rate, **OERE**: Oxygen Evolution Reaction Efficiency, **DMF1:** dimethylformamide synthesis first, **DMF2:** dimethylformamide synthesis second, **DMF3:** dimethylformamide synthesis Third, **BB**: *Bacillus benzeovorans*, **EC**: *E. coli,* **DD**: *Desulphovibrio Desulphuricans*, **GC MS**: Gas Chromatography coupled Mass spectrometry, **GC FID**: Gas Chromatography coupled Flow Injection Detecter.

Note: References as mentioned in the main manuscript.

SD1. Tables regarding bioactive and catalytic of Ru-cNMs reported till 2019

Table 1: Ru based nanomaterials synthesized through bioextracts, and their Biological characterizations

Category	Shrivastav *et al.* (2012)	Gopinath *et al.* (2014)	Kannan *et al.* (2015)	Ali *et al.* (2017)
Reducing entity	Bacteria(G-), *Pseudomonas aeruginosa* SM1	Plant (Angio.), *Gloriosa superba*	Plant (Angio.), *Acalypha Indica*	Algae, *Dictyota dichotoma*
Phylogeny	Pseudomonadaceae	Lilliaceae	Euphorbiaceae	Dictyotaceae
Part used	extracellular layers	Dried Leaves	Dried Leaves	Leaves & stems
Solvent	Aqueous	Aqueous	Aqueous	Aqueous
[Electrolyte]	$(NH_4)_2[RuCl_6]$, 1 mM, 50 mL	$RuCl_3.xH_2O$, 2mM, 100 mL	$RuCl_3.xH_2O$, 0.1 M, 50 mL	Ru aq. solution, 2 mM, 90 mL
Ext. prepar-ation	Nutrient broth, 27 °C, 120 rpm	0.1 g/mL, 50-60 °C, 5 min	0.2 g/mL, 50-60 °C, 30 min	Known weight, heated for 5 min
[Ext.] used	0.2 g cell pellet	1 mL	10 mL	10 mL
Temp (°C), duration	RT, 24 h	100, 20 min	80, 2 h	RT, 10 min
Stir (rpm), duration	Static	Stirred	1000, 10 min	12000, 20 min
Calcination	N/D	N/D	At 600 °C	N/D
NPs type	Ru NPs	Ru NPs	RuO_2 NPs	Ru NPs
NPs size (nm)	2.9-13.7	25-90	6-25	25-90
Dispersity	PD	PD	PD	PD
Lattice	N/D	Hexagonal	Orthorhombic	Cubic, FCC
Agglomerate	No	Yes	Yes	No
Nature	Amorphous	Crystalline	Crystalline	Crystalline
Shape	Spheres and Disc	Spherical	Irregular	Irregular
Bioactivity	N/A	Antibacterial activity (against *P. aeruginosa, E. coli, S. aureus, S. pneumoniae, B. subtilis*)	Antibacterial activity (against *E. coli, P. aeruginosa, S. aureus, S. marcescens*)	Anticancer activity estimated against HeLa, MCF-7, ad VERO cell line.
Synthesis Mechanism	1°/2° amine mediated reduction	Phenolics oxidation	Quinol/quinone conversion	N/D
References	[7]	[8a]	[8b]	[8c]

Table 1: Ru based nanomaterials synthesized through bioextracts, and their Biological characterizations (cont.)

Category	Gupta *et al.* (2019)			
Reducing entity	Plant (Pterido.), *Nephrolepis biserrata* Furcans	Plant (Gymno.), *Cycas revoluta*	Plant (Angio.), *Catharanthus roseus*	Plant (Angio.), *Ocimum sanctum*
Phylogeny	Nephrolepidaceae	Cyacadaceae	Apocynaceae	Labiatae
Part used	Fresh Leaves	Fresh Leaves	Fresh Leaves	Fresh Leaves
Solvent	Methanolic	Methanolic	Methanolic	Methanolic
[Electrolyte]	$RuCl_3.xH_2O$, 2.4 mM, 40 mL	$RuCl_3.xH_2O$, 2.4 mM, 40 mL	$RuCl_3.xH_2O$, 2.4 mM, 40 mL	$RuCl_3.xH_2O$, 2.4 mM, 40 mL
Ext. prepar-ation	0.125 g/mL, 50 °C, 10 min	0.125 g/mL, 50 °C, 10 min	0.125 g/mL, 50 °C, 10 min	0.125 g/mL, 50 °C, 10 min
[Ext.] used	0.5 mL	0.5 mL	0.5 mL	0.5 mL
Temp (°C), duration	50, sand bath, 35 min	50, sand bath, 35 min	50, sand bath, 35 min	50, sand bath, 35 min
Stir (rpm),	17800, 15 mins	17800, 15 mins	17800, 15 mins	17800, 15 mins

duration				
Calcination	N/D	N/D	N/D	N/D
NPs type	Ru NPs	Ru NPs	Ru NPs	Ru NPs
NPs size (nm)	25.96	26.52	19.63	20.92
Dispersity	MD	MD	MD	MD
Lattice	Cubic, Primitive	Cubic, Primitive	Cubic, Primitive	Cubic, Primitive
Agglomerate	No	No	Yes	No
Nature	Amorphous	Polycrystalline	Crystalline	Polycrystalline
Shape	Hexagonal	Spherical	Irregular	Orthorhombic
Bioactivity	Significant Antifungal activity (against *A. flavus*)	Minor Antifungal and antioxidant activity	Significant Antioxidant activity (DPPHS, ABTSS, SORS, HSA)	Significant Antioxidant activity (DPPHS, ABTSS, SORS, HSA)
Synthesis Mechanism	Flavonoid redox reaction	Flavonoid redox reaction	Flavonoid redox reaction	Flavonoid redox reaction
References	[9]			

Table 2: Ru based nanomaterials synthesized through bioextracts, and their Catalytic Potency

Category	**Huang *et al.* (2014) BTC**	**Huang *et al.* (2015) MTS**	**Ismail *et al.* (2016) WSR**	**Ismail *et al.* (2016) SCE**	**Zhang *et al.* (2016) NTA**	**Sano *et al.* (2016) MFC**
Reducing entity	Plant (Gymno.), *Cacumen platycladi*	Plant (Gymno.), *Cacumen platycladi*	Plant (Angio.), *Aspalathus linearis*	Plant (Angio.), *Aspalathus linearis*	Plant (Angio.), *Diospyros kaki*	Bacteria (G-), *Shewanella algae*
Phylogeny	Cupressaceae	Cupressaceae	Fabaceae	Fabaceae	Ebenaceae	Shewanellaceae
Part used	Dried Leaves	Dried Leaves	Dried Leaves	Dried Leaves	Dried Leaves	Cultured microbe
Solvent	Aqueous	Aqueous	Aqueous	Aqueous	Aqueous	Aqueous
[Electrolyte]	$RuCl_3.xH_2O$, 50 mL, 2.2 mM, @(stir) 60°C, 1 h	$RuCl_3.xH_2O$, 50 mL, 2.2 mM, @(stir) 60°C, 1 h	$RuCl_3.xH_2O$, added 6.0 g, pH maintained at 3.8	$RuCl_3.xH_2O$, added 6.0 g, pH maintained at 3.8	0.5 mM $RuCl_3.xH_2O$+ 0.5 mM $H_2PtCl_6.6H_2O$ (40 mL), @(stir) RT, 1 h	4.3 mM, 5 mL $RuCl_3.xH_2O$+ 5 mM, 15 mL $H_2PtCl_6.6H_2O$ (40 mL), @(stir) RT, 1 h
Ext. prepara-tion	Milling of plant powder, 0.01 g/mL, Stir, RT, 4h	Milling of plant powder, 0.01 g/mL, Stir, RT, 4h	1.6 x 10^{-4} g/mL, pH: 3, heat, 3 h, SF	1.6 x 10^{-4} g/mL, pH: 3, heat, 3 h, SF	Milling plant powder, 0.067g/mL, stored at 4°C	*S. algae* (ATCC51181) grown in TSB (aerobic)
[Ext.] used	30 mL	30 mL	300 mL	300 mL	25 mL	N/D
Substrate used	CNT, opt amt., heated with Ru solution, 60°C, 1 h	AC, opt amt., added after 0.5 h of the above reaction	Electrodeposition of NPs on Cu_2O substrate due to its excitation energy of 2.1 eV	NiF (BD 450 g/m^2, P: 95%, 1.6 mm thick), EtOH- Ru NPs doped over NiF, dried at 60°C, ½ h	HNO_3 treated CB, opt amt., added after the reaction, stir, RT, 1 h	CB,1:1(algae:CB) A. Ext. added to Pt^{+4}+Ru^{+3}. B. Ru^{+3} added to Pt^{+4}+Ext. Rate: 1cm^3/h
Temperature (°C), duration	60°C, 5 h. vaccum dried at 60°C:12 h	60°C, 5 h. vaccum dried at 60°C: 12 h	RT, 2 h, heat at 90 °C, for 1h	RT, 2 h, heat at 90 °C, for 1h	RT, 2 h	pH: 7 via H_3PO_4 buffer, 50 mol/mL COONa added to Pt^{+4} soln.
Stir (rpm), duration	Stir, 5 h	Stir, 5 h	1000, 3 times, 10 min each	1000, 3 times, 10 min each	Stir, 2 h	NPs Electrode in DMFC and

						compared
Calcination/ Anealling	500°C, 3 h, N_2 atmosphere	500°C, 3 h, N_2 atmosphere	Anealling for 2 h at 400 °C	Anealling for 2 h at 400 °C	300°C, 2 h. Reduced with H_2 at 250°C for 3 h	N/A
S_{BET} (m^2/g)	197	949	137.1	N/D	878	N/D
V_p (cm^2/g)	0.93	0.94	N/D	N/D	0.35	N/D
R_p (nm)	18.6	0.4	N/D	N/D	5.6	N/D
NPs type	Ru NPs@CNT catalyst	Ru NPs@AC catalyst	RuO_2 NPs@Cu_2O/ ITO-Gs	RuO_2 NPs@NiF	$Ru_{0.5}Pt_{0.5}$ NAs@OAC	Pt_xRu_{1-x} NAs@CB
NPs/NCs size (nm)	3.3-5.5	2.17	1.4-1.3	5	4-11 (Avg. 7.21)	<5 nm
Dispersity	PD	MD	PD	MD	PD	MD
Lattice	N/D	N/D	Rutile	N/D	N/D	Hexagonal
Agglomerate	No	No	No	No	No	No
Nature	Amorphous	Amorphous	Amorphous	Amorphous	Single-phase Crystalline	Crystalline
Shape	Spherical	Irregular	Spherical	Spherical	Quasi-spherical	Ellipsoidal
Synthesis Mechanism	Redox Mechanism	Redox Mechanism	Quinol/quinone conversion	Quinol/quinone conversion	Redox mechanism	Redox mechanism
Catalysis	Catalytic reduction of Benzene to cyclohexane	Catalytic reduction of maleic acid to succinic acid	Water Splitting Reaction	Supercapacitor and electrode	Catalytic reduction of *o*-chloronitro-benzene to *o*-chloroanilline	Used in as anode in DFMC
Catalysis conditions	Ru loading 2% (w/w): 0.05 g, 80°C, 4 MPa N_2 , 0.5 h, solid state synthesis.	Ru loading 2% (w/w): 0.05 g, 150°C, 6 MPa H_2, 0.5 h, Solvent: THF.	Electrode:Ru over Cu_2O coating over ITO layer over the glass surface.	Electrode prepared for this material.	0.5 g of 1:1 (Ru:Pt), 50°C, 1 MPa H_2	Incorporated in electrodes of DMFC with CB, RT
Catalytic efficiency	Conversion: 99.97% TOF: 6983/h Recycle: 6 times	Conversion: 99.4% Selectivity: 99.6% TOF: 2084.9/h Recycle: 5 times	Stoichiometric amounts of H_2& O_2 in 227 h	97% of capacitance lost after 500 charge/discharge cycles.	Conversion: 99.8% Selectivity: 98.4% Rate: 0.26 Recycle: 5 times	A. Poisoning reactivated after 10 min, avg. potential 0.04 V B. Pt poisoning
References	[59a]	[59b]	[45a]	[10]	[56]	[11]

Table 2: Ru based nanomaterials synthesized through bioextracts, and their Catalytic Potency(Cont.)

Category	**Yu *et al.* (2019) WSR**	**Omajali *et al.* (2019) DMF1**	**Mikheenko *et al.* (2019)DMF2**	**Bolivar *et al.* (2019) DMF2**
Reducing entity	Fungi, *Saccharomycete* sp.	Bacteria (G+) *Bacillus benzeovorans*	Bacteria (G-) *Desulphovibrio desulphuricans*	Bacteria (G-) *Escherichia coli* MC4100
Phylogeny	Saccharomycetaceae	Bacillaceae	Desulphovibrionaceae	Enterobacteriaceae
Part used	Dried cell mass	Dried cell mass	Dried cell mass	Dried cell mass
Solvent	Aqueous	Aqueous	Aqueous	Aqueous
[Electrolyte]	0.1 M, 0.5 mL $RuCl_3.xH_2O$ added to the *Saccharomycete* cell solution	2 mM H_2PdCl_4 + 1 mM $RuCl_3.xH_2O$ (pH=2, 10mM HNO_3)	2 mM H_2PdCl_4 + 1 mM $RuCl_3.xH_2O$ (pH=2, 10mM HNO_3)	2 mM H_2PdCl_4 + 1 mM $RuCl_3.xH_2O$ (pH=2, 10mM HNO_3)

Ext. preparation	3.33 x 10^{-3} g/mL *Saccharomycete* cells		Strain grown to OD_{600}:0.7-1.0, centrifuge:9000 g, 15 min, 4°C.	Strain grown to OD_{600}:0.7-1.0, centrifuge:9000 g, 15 min, 4°C.	Strain grown to OD_{600}:0.7-1.0, centrifuge:9000 g, 15 min, 4°C.
[Ext.] used	30 mL		As per (% w/w) ratio	As per (% w/w) ratio	As per (% w/w) ratio
Substrate used	N/P Doped Carbon substrate		Cell biomass was used as NPs support	Cell biomass was used as NPs support	Cell biomass was used as NPs support
Temperature (°C), duration	Gentle heating at 30° C, 24 h to form grey Ru-*Saccharomycete* cell		30°C, 96 h	30°C, 96 h	30°C, 96 h
Stir (rpm), duration	Stir under dark for 24 h		180 rpm	180 rpm	180 rpm
Calcination/ Anealling	Ar/H_2 environment, at 900°C rate: 2°C/min, , 2 h	Aerial, at 500°C rate: 2°C/min, 2 h	N/D	N/D	N/D
S_{BET} (m^2/g)	617.85	166.34	N/D	N/D	N/D
V_p (cm^2/g)	N/D		N/D	N/D	N/D
R_p (nm)	N/D		N/D	N/D	N/D
NPs type	Ru/Ru_2P NPs@NPC	RuO_2 NPs NPs@NPC	RuPd NPs@EC	RuPd NPs@DD	RuPd NPs@BB
NPs/NCs size (nm)	7000-6000	2000-3000			2-3 nm
Dispersity	PD		PD	PD	PD
Lattice	Ru: Hexagonal Ru_2P: orthorhombic	Rutile	N/D	N/D	N/D
Agglomerate	No		Occasionally	Occasionally	Occasionally
Nature	Crystalline	Polycrystalline	Amorphous	Amorphous	Amorphous
Shape	Spherical		Mixed	Mixed	Mixed
Synthesis Mechanism	Redox mechanism		Bioreduction and redox mechanism	Bioreduction and redox mechanism	Bioreduction and redox mechanism
Catalysis	Catalyze Water Splitting Reaction in acidic medium		Catalyze conversion of 5-hydroxymethyl furfural (HMF) to 2,5-dimethyl furfural (DMF)	Catalyze conversion of 5-hydroxymethyl furfural (HMF) to 2,5-dimethyl furfural (DMF)	Catalyze the up-gradation of 5-hydroxymethyl furfural (HMF) to 2,5-dimethyl furfural (DMF) obtained from biowastes.
Catalysis conditions	0.5 M H_2SO_4 soln.,		2.5:1 (w/w) 5-HMF:catalyst, H_2 purge, H_2 pressure (50 bar), 2h, 260°C, 500 rpm, stored at -20°C, filtered, GC-FID, GC-MS	2.5:1 (w/w) 5-HMF:catalyst, H_2 purge, H_2 pressure (50 bar), 2h, 260°C, 500 rpm, stored at -20°C, filtered, GC-FID, GC-MS	2.5:1 (w/w) 5-HMF:catalyst, H_2 purge, H_2 pressure (50 bar), 2h, 260°C, 500 rpm, stored at -20°C, filtered, GC-FID, GC-MS
Catalytic efficiency	HERE: high, Op: 42 mV@10 mA cm^{-2} ,CD: 1000 mA cm^{-2}, Tafel Slope: 37.5 mV dec^{-1}	OERE: medium, Op: 220 mV@10 mA cm^{-2} ,CD: 1000 mA cm^{-2}, Tafel Slope: 66.8 mV dec^{-1}	Conversion: 100% Selectivity: <50%	Conversion: 100% Selectivity: <50%	Conversion: 100% Selectivity: >50%
	Cell Notation: Ru/Ru_2P NPs@NPC(-) II RuO_2 NPs@NPC(+) Needed 1.5 V to attain 10 mA cm^{-2}				

References	[55]	[19a]	[104]	[19b]

SD2. Table depicting tentative synthesis mechanism of green Ru-cNMs

Table 3: Plant extract based synthesis of Ru-cNMs and tentative mechanism for their reaction

S.No.	Ru-cNMs	Plant Extract	Tentative synthesis strategy	Ref.
1.	Ru NPs	*Gloriosa superba* (Aqueous)	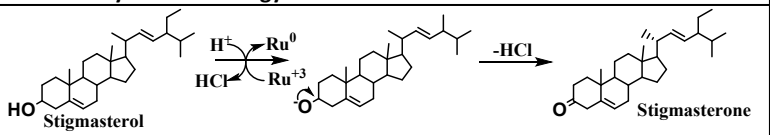	[8a]
2.	RuO_2 NPs	*Acalypha indica* (Aqueous)	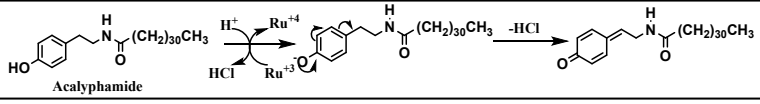	[8b]
3.	Ru NPs	*Dictyota dichotoma* (Aqueous)	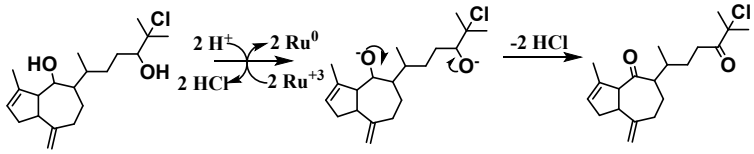	[8c]
4.	Ru NPs	*Catharanthus roseus* (Methanolic)	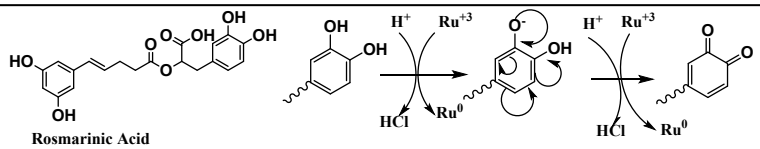	[11]
5.	Ru NPs	*Ocimum tenuiflorum* (Methanolic)	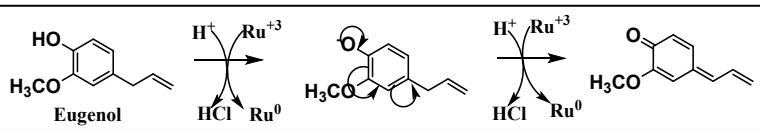	[11]
6.	Ru NPs	*Nephrolepis biserrata* (Methanolic)	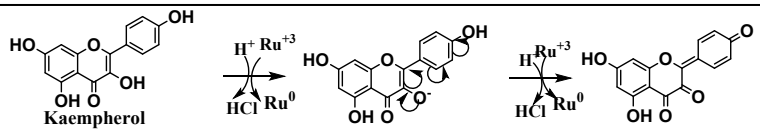	[11]
7.	Ru NPs	*Cycas revoluta* (Methanolic)	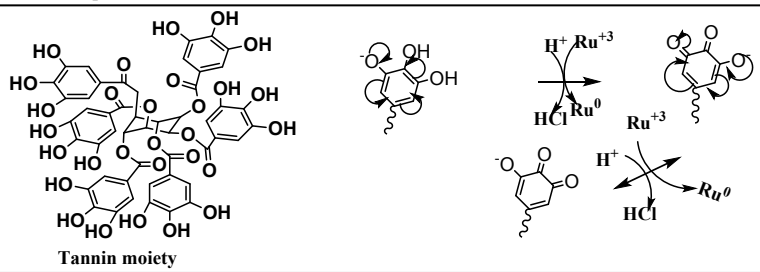	[11]
8.	Ru NPs@AC and Ru NPs@CNT	*Cacumen platycladi* (Aqueous)	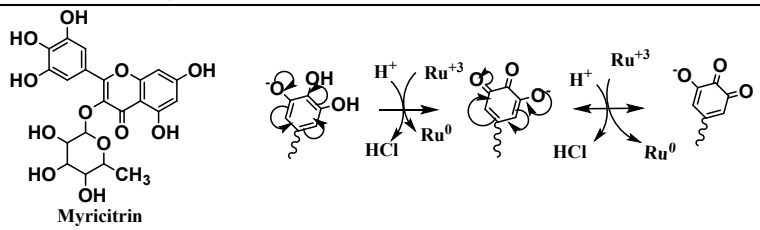	[59]
9.	$Ru_{0.5}Pt_{0.5}$ NPs @OAC	*Diospyros kaki* (Aqueous)	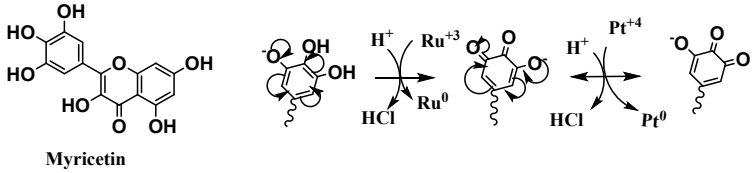	[56]

10.	RuO_2 NPs	*Aspalathus linearis* (Aqueous)	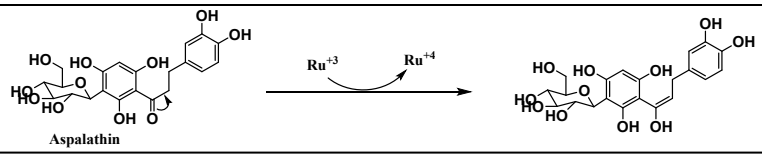 Aspalathin	[45a]

SD3. Tauc's Relation and calculation of Optical band gap

Absorption coefficient (ε) and Optical density (OD=α=ε.c, where c is the concentration of NPs solution) for the vortexed solution of amorphous NPs are used to calculate optical band gap (E_g) by knowing the photonic energy ($h\nu$) as,

$$[(\alpha - \alpha_s)h\nu]^{1/n} = \beta(h\nu - E_g)$$

which is called Tauc relation, where α_s is the minimum absorption coefficient of solvent, β is band tailing parameter, and n is power factor (equivalent to 1/2, 3/2, 2, or 3 for direct allowed, direct forbidden, indirect allowed and indirect forbidden transitions) respectively [70]. Tauc plots, drawn between $[(\alpha - \alpha_s)h\nu]^{1/n}$ and $h\nu$, for different values of n and their extrapolation up to $[(\alpha - \alpha_s)h\nu]^{1/n}$ = 0 is used to deduce E_g and β for these transitions.

SD4. Atomic Surface Concentration Ratio (ASCR)

Atomic surface concentration ratio (ASCR) can be semi-quantitatively calculated as,

$$\frac{C_O}{C_{Ru}} = \frac{A_O/S_O}{A_{Ru}/S_{Ru}}$$

where C is the atomic surface concentration of the given species, A is absorption peak width for a particular species, and S is the sensitivity with respect to the orbitals of a particular atom (for O 1s S_O =2.93, and for Ru $3d_{5/2}$ S_{Ru} =7.39).

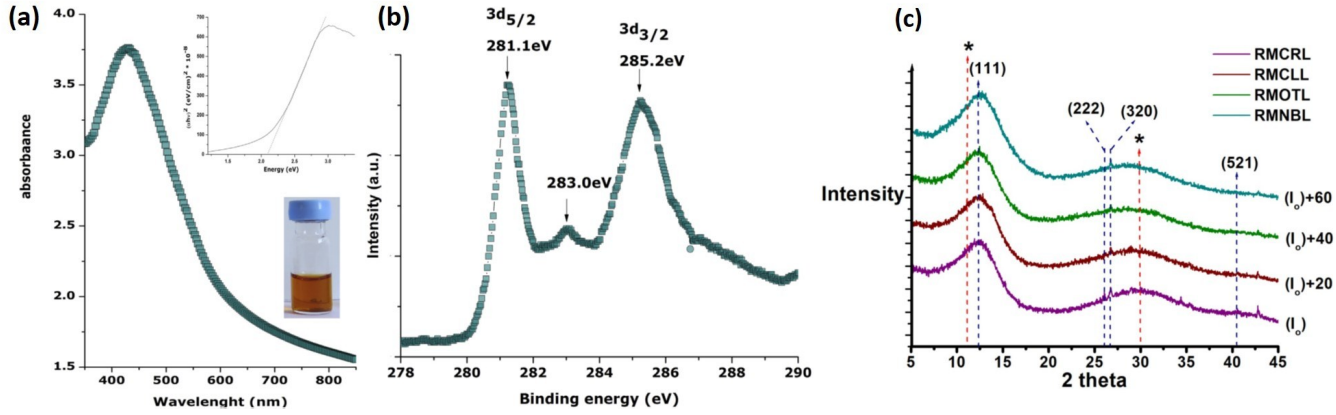

Figure 1: (a, b) UV-Vis-NIR (with Tauc plot as inset)and Ru core XPS spectra of RuO_2 NPs synthesized using aqueous leaf extracts of *Aspalathus linearis* [45a] **(c)** Powder XRD spectra of Ru NPs(RCRL, RMOTL, RMCLL, and RMNBL) synthesized using methanolic extracts of *Catharanthus roseus*, *Ocimum tenuiflorum*, *Cycas revoluta*, and *Nephrolepis biserrata* respectively [9]

SD5. Williamson Hall Equation

XRD methods use Debye Scherrer formula for particle size calculation owing to particle size broadening

$$\theta_{sz} = 0.9\lambda / D \cos\theta$$

However, Ru NPs being synthesized from plant extracts are smaller in size (<10 nm) and have high surface activity, owing to which they offer non-ideal peak broadening complicating deduction of crystal parameters. This additional peak broadening owing to excessive shear strain ($\theta_{st} = 4\,\varepsilon \tan\theta$) can be dealt through the Williamson Hall plot i.e., the plot of $\beta_{tot}\cos\theta$ against $C\sin\theta$, in accordance to,

$$\beta_{tot}\cos\theta = {K\lambda}/{D} + (C\sin\theta)\varepsilon$$

where, β_{tot}, θ, λ, D, and ε are total peak broadening (rad), Bragg's diffraction angle, wavelength (1.540 A°), particle size (A°), and shear strain. *K* and *C* are constants equal to 0.9 and 4.00 respectively. The plot has been used to calculate *D* and ε.

$$\beta_{tot}\cos\theta = {K\lambda}/{D} + \left({C\sin\theta}/{E_{hkl}}\right)\sigma$$

$$\beta_{tot}\cos\theta = {K\lambda}/{D} + \left(C\sin\theta\sqrt{\frac{2}{E_{hkl}}}\right)\sqrt{u}$$

Furthermore, the magnitude of strain can be used to calculate stress(σ), and energy density(u) if the value of Young's Modulus (E_{hkl}) is known. This strain originated deviation can be deduced through the Williamson Hall plot. The magnitude of deviation obtained for ZnO and RuO_2 NPs has been used to calculate particle size, stress, and energy density of NPs. Uncalcined RuO_2 NPs show rutile structure, with undefined lattice. On calcination, NPs re-nucleate with a homogeneous lattice. Band displacement and reduction of lattice parameters confirm the synthesis of bimetallic NPs. The presence or absence of Ru broad peak at 43° is dependent on alloying efficiency. Presence of this peak in Ru_xM_x systems confirms the partial dissolution of metal (M) into Ru lattice. RuPt NPs of this type show minor peaks confirming Ru-Pt alloying. In Ru_xM_y (Ru_xPt_y) systems these characteristics aren't visible, confirming the

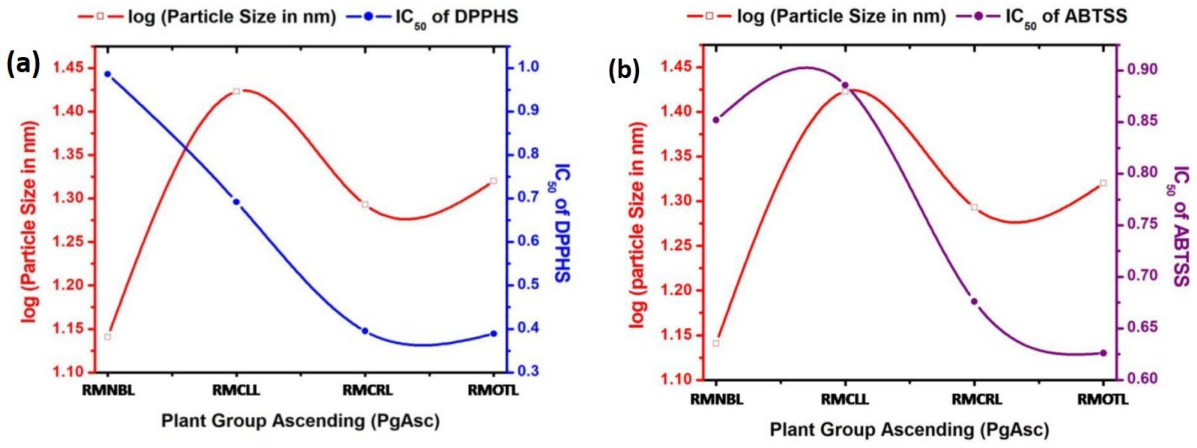

Figure 2: Nanoparticle-Plant group correlation Plot of Ru NPs(RCRL, RMOTL, RMCLL, and RMNBL) synthesized using methanolic extracts of *Catharanthus roseus*, *Ocimum tenuiflorum*, *Cycas revoluta*, and *Nephrolepis biserrata* repersenting **(a)** DPPH scavenging and **(b)** ABTS scavenging assays [9]

presence of metallic Ru metal and unalloyed metal NPs. In mixed (Ru_xM_x+Ru_xM_y) systems broadband of Ru may or may not be visible depending upon alloying efficiency.

SD6. X-Ray Absorption Spectroscopy and X-ray Absorption Near Edge Spectroscopy (XAS and XANES)

Dry samples of metal NPs, are analysed and processed using ATHENA code with eradiation of background through pre-edge linear function. EXAFS fitting is done via a shift in threshold energy and amplitude factor, as a universally fixed parameter, using FEFF8 calculations. In the case of Ru NPs, RuO_2, $RuCl_3$, and Ru foil are used as reference materials. FEFF8 calculations of Pd-K edge data revealed the tetragonal PdO like crystal structure of Pd coordinated with 2 different oxygen atoms (with bond lengths 2.1 and 2.5 A^o) of biological origin (particularly of Asp or Glu residues of capping proteins), and with another four distinct Pd atoms (with bond length varying from 2.74 to 5.40 A^o). Similar calculations revealed the both metallic Ru and RuO_2 shells were indistinguishably present in NPs with 1 Ru-Ru bond and 2 distinct Ru-O bonds (of bond lengths 1.96-2.04 and 2.10-2.16 A^o respectively), originated from RuO_2 and $Ru(OH)_3$, respectively. However, the geometry of Ru centre remained undefined due to nearly similar atomic number of Ru and Pd and low concentration of Ru in RuPd NPs.

SD7. Electron Diffraction Spectroscopy (EDAX)

As per Bolivar *et al.*Elemental mapping of low Ru concentration confirmed uniform distribution of Pd, surface enrichment of Ru, and intracellular deposition of Ru NPs. They showed the presence of Pd(0) [111] lattice fringes(0.24 nm), but no defined fringes of Ru owing less Ru to Pd association in NPs. High Ru concentration bio RuPd NPs had both small and large-sized intracellular NPs, the later containing Pd. These bimetallic NPs showed core-shell and dumbell shell the structure with Pd(0) [111] lattice fringes(0.236 nm), RuO_2 [110] lattice fringe (0.231 nm) and Ru(0)[101]/RuO_2[210] lattice fringe(0.201 nm). Unlike high contrasting Z images of AuPd NPs (Z_{Au} = 79, Z_{Pd} = 46), Z images of RuPd NPs (Z_{Ru} = 44) are of low contrasts owing to similar atomic numbers of Ru and Pd.

SD8. Brunauer Emmet Teller (BET) plots and measurement of other surface parameters

BET surface area is estimated through N_2 physisorption process in accordance with the formula,

$$\frac{p}{v(p_o - p)} = \frac{1}{v_m c} + \left(\frac{c-1}{v_m c}\right)\frac{p}{p_o}$$

Where *p, p_o, v, v_m,* and *c* are, sample's vapour pressure, solvent's vapour pressure, adsorbent's volume, monolayer volume and a relative lifetime of states ($e^{(E-L)/RT}$, *E* and *L* are enthalpy of adsorption and latent heat of condensation) respectively. The plot of relative partial pressure (p/p_o) against the pressure fraction (i.e. $\frac{p}{v(p_o - p)}$) has been used to estimate *c* and v_m. Specific surface area ($S_{BET} = \frac{v_m N_a A_{cs}}{M\,w}$) can be estimated whereby, N_a, A_{cs}, *M,* and *w* are Avogadro's number (6.02 x 10^{23}), cross-sections area of adsorbate (16.2 A$^{o\ 2}$ for N_2), the molecular weight of adsorbate (28.0134 g/mol for N_2), and sample weight respectively. Detailed knowledge of isotherms have been used to calculate pore volume ($V_p = \frac{P_a v_m V_M}{R\,T}$), pore radius ($R_p = \frac{2V_p}{S}$), whereby, P_a, V_m, *R, T,* and *S* are ambient pressure, molar volume, gas constant, ambient temperature, and total surface area (S_t=S_{BET} x *w*). Carbon nanotube (CNT) doped green Ru-cNMs have shown type IV adsorption isotherm with a decrease in S_{BET} and V_p, confirming their

mesoporous nature. An increment of R_p from 15.3 to 19.7 nm is attributed to concentration-based, pore extension ability of these NPs

SD9. Electrochemical measurements

The working potential of metal NSs electrode can be estimated through Galvanostatic Charge Discharge (GCD) measurements, within a suitable potential range, carried over various current densities. The shape of the galvanostatic charge-discharge curve can be used to coin the energy storage mechanism in supercapacitive systems. Capacitors show a sharp decrement in their potential with the lowest potential limit of 0 V, i.e., for such systems, $V_1>V_2$, and $V_2=0$. Unlike this, Pseudo-capacitors systems give show a decremental curve only after a consistent potential plateau, even at different current densities with low iR drop, such that the lowest potential limit is never equal to zero, i.e, for these systems, $V_1>V_2$, but $V_2\neq0$. Owing to its recurrent adsorption-desorption activity, transition metal NPs mostly show pseudocapacitive behaviour. Specific capacitance (*C*), i.e., capacitance offered per mg of Ru-cNMs (F mg^{-1}) can be calculated from,

$$C = \frac{(\Delta Q/\Delta V)}{w} = \frac{I\,\Delta t}{w\,\Delta V}$$

where, *Q, I,* Δt*, w,* and ΔV are charging-discharging charge(mC), charge-discharge current(mA), discharging time(s) and amount of metal NSs(mg). The gradual decrease in specific capacitance on increasing current density can be attributed to insufficient and incremental potential drop along with the involvement of active material in redox reactions at higher charge densities. This technique is also a semi-qualitative confirmation of NSs-substrate interaction and NPs's supercapacitive nature.

Randles electronic equivalent circuit consisting of combined series resistance (R_s) corresponding to electrode's ionic resistance and contact resistance at active substance/current collector interface, and a parallel combination of charge transfer resistance (R_{ct}) and constant phase element (CPE). CPE includes both, the double layer electrode capacitance and ideal polarizable capacitance. The real to imaginary intersection point at high frequency and slope of the Nyquist plot at low frequency corresponds to R_s and W respectively. The actual deviation found between real and imaginary impedance is attributed to the additional Warburg resistance (W) owing to the diffusion of counterion. Low R_s and low R_{ct} values confirm the biosynthesis strategy and good electrical conductivity of Ru-cNMs. Impedance of the constant phase element of Randles's circuit (Z_{CPE}) can be calculated from:

$$Z_{CPE} = \frac{1}{D(k\omega)^n}$$

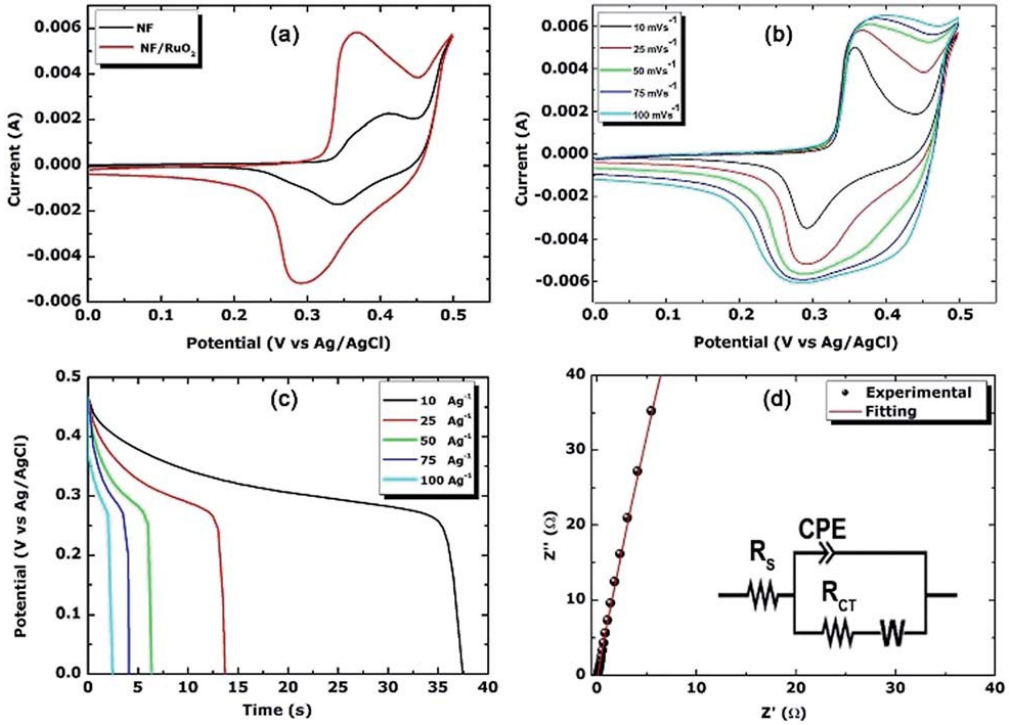

Figure 3: (a, b) Cyclic Voltametric spectra of RuO_2 (RuO) and NiF coated RuO_2 NPs over various scan rates **(c)** Galvanostratic Charge/Discharge (GCD) plots over various NPs concentration (in grams) **(d)** Experiment(dot) and fitted(red line) Nyquist Plot and Randle's equivalent circuit for RuO_2 NPs synthesized using aqueous extract of *Aspalathus linearis* [10]

where, *D, k,* ω*,* and *n* refers to the combined surface and electroactive property coefficient, capacitive (C) or inductive (L) magnitude, angular frequency and capacitor kinetics-electrode roughness correlation factor, respectively. Value of *n* can vary from 1 (for ideal capacitor) to -1 (for ideal inductor). Value of *n* corresponds to 0 for an ideal resistor, and 0.5 is assigned to diffusion phenomena Photoreduction efficiency is measured using gas chromatographic techniques.

SD10. Electronic Setup of Direct Methanol Fuel Cell (DMFC)

Ru-Pt DMFC systems, proposed for preventing CO mediated Pt inactivation, have been prepared and tested through experimental DMFC setup. In this cell, crushed reductant carbon paper mixture in the ratio of 1:2 was prepared and used for preparing electrodes, which were separated by proton conductive solid media like Nafion117 membrane. The membrane electrode assembly (MEA) was prepared by hot-pressing. The MEA and Nafion117 membrane was sandwiched by acrylic plates. DMFC anodes and cathodes were continuously supplied by fuel, (i.e., aqueous methanol in this case), and ambient air. The open-circuit voltage between these electrodes was monitored through a digital multimeter for estimating the extent of Pt inactivation.